

On the through-thickness critical current density of an $\text{YBa}_2\text{Cu}_3\text{O}_{7-x}$ film containing a high density of insulating, vortex-pinning nanoprecipitates

S. I. Kim,^{a)} F. Kametani, Z. Chen, A. Gurevich, and D. C. Larbalestier
*Applied Superconductivity Center, National High Magnetic Field Laboratory, Florida State University,
 Tallahassee, Florida 32310*

T. Haugan and P. Barnes
Air Force Research Laboratory, Dayton, Ohio 45433

(Received 14 March 2007; accepted 24 May 2007; published online 18 June 2007)

Using sequential ion milling the authors have studied the thickness dependence of the critical current density $J_c(H)$ of a single crystal $1\ \mu\text{m}$ thick $\text{YBa}_2\text{Cu}_3\text{O}_{7-x}$ thin film containing $\sim 5\ \text{vol}\%$ of insulating Y_2BaCuO_5 (Y211) nanoparticles in order to better understand how to obtain high critical currents in thick films. Except very near the interface where the defect density was enhanced, $J_c(H)$ in the body of the film was uniform and independent of thickness with a high maximum pinning force of $8.8\ \text{GN}/\text{m}^3$ at $77\ \text{K}$. The authors conclude that the nanoscale Y211 precipitates result in strong, three-dimensional pinning characterized by a pin spacing of $\sim 30\ \text{nm}$, much smaller than the film thickness. © 2007 American Institute of Physics. [DOI: 10.1063/1.2749437]

$\text{YBa}_2\text{Cu}_3\text{O}_{7-\delta}$ (YBCO) is a very versatile superconductor into which many types of vortex-pinning centers can be introduced.^{1–6} As the limits to the current-carrying capability of this technological compound are explored, the commonly observed decline of J_c with increasing film thickness t (Refs. 7–12) is still not well understood. Such a thickness dependence may result from the transition from the two-dimensional pinning of rigid vortex lines in thinner films to the three-dimensional (3D) pinning of deformable vortices even for a completely uniform pinning nanostructure.^{13,14} However, there are also many reports of microstructures varying across YBCO films, which can also cause a thickness-dependent $J_c(t)$. For example, Foltyn *et al.*,¹⁵ who studied single crystal YBCO films grown by pulsed laser deposition (PLD) without any added second phase, found that the thickness dependence of the average J_c can result from a decrease of the local J_c , out to a t of $\sim 0.65\ \mu\text{m}$, followed by a thickness-independent J_c . They ascribed the high J_c at the interface at the CeO_2 cap layer to a $20\ \text{nm}$ thick caging array of interface dislocations which strongly enhance local vortex pinning.

We recently investigated the thickness dependence of J_c in YBCO coated conductors made by the metal organic deposition (MOD) process and found no evidence for dimensional pinning crossover as the reason for the observed decline of J_c with increasing t .¹⁶ Analysis of the thickness dependence of $J_c(H)$, the normal state resistivity, and the microstructure showed that MOD films exhibit microstructural degradation which grows as the films thicken, producing a thickness-dependent reduction of the effective current-carrying cross section A_{eff} . High angle grain boundaries,^{17–21} porosity,^{12,16} insulating phases,²² or other macroscopic planar obstacles²³ reduce the cross section for current flow. In fact, the MOD films exhibited both strong single vortex pinning and a thickness-dependent porosity, which together result in the quasilinear decay of the average J_c with increasing t .

To better test the physical mechanisms at play, we have studied the thickness dependence of J_c in a PLD YBCO film to which insulating Y_2BaCuO_5 (Y211) particles were delib-

erately added. Our hypothesis was that the addition of insulating nanoparticles should yield a thickness-independent J_c , since strong pins should enable each vortex segment to be pinned independently. In this letter, we show that such precipitates do take YBCO into the very desirable strong 3D pinning regime, in which the longitudinal pinning correlation length is much shorter than the film thickness, and the local J_c is then independent of t . In principle, this permits a high and a thickness-independent J_c in thick films, provided that thickness degradation of the current-carrying cross section and variation of the second-phase vortex-pinning structure are avoided.

An YBCO film was deposited by PLD on a single crystal SrTiO_3 substrate. The Y211 nanoparticles were introduced by alternate deposition of Y211 ($\sim 0.8\ \text{nm}$) and YBCO ($\sim 16.5\ \text{nm}$).¹ A $50\ \mu\text{m}$ wide $\times 400\ \mu\text{m}$ long bridge was patterned and was then sequentially thinned with $500\ \text{eV}$ Ar ions impinging at 45° while the sample was cooled to $\sim 230\ \text{K}$. After each milling step, $J_c(H)$ was measured ($1\ \mu\text{V}/\text{cm}$ criterion) at $77\ \text{K}$ for magnetic fields up to $10\ \text{T}$ applied perpendicular to the film surface. The full thickness of the YBCO was $1.0\ \mu\text{m}$, and the thickness of each thinned sample was measured with a Tencor profilometer. Cross-section transmission electron microscopy (TEM) imaging was performed in a Philips CM200UT.

This sample exhibited a full-thickness $J_c(0\ \text{T}, 77\ \text{K})$ of $3.4\ \text{MA}/\text{cm}^2$, T_c of $90.0\ \text{K}$ defined at the onset of resistance, and an irreversibility field $H_{\text{irr}}(77\ \text{K})$ of $8.8\ \text{T}$ measured at $J_c = 100\ \text{A}/\text{cm}^2$. The maximum pinning force $F_{p,\text{max}}$ was $\sim 8.8\ \text{GN}/\text{m}^3$.

Figure 1 shows the $J_c(t)$ data as a function of the residual thickness for each milling step. The critical current per unit width I_c^* shown in the inset of Fig. 1 exhibits a linear dependence on t , which extrapolates to a nonzero value of I_c^* at zero t . Such a linear dependence is inconsistent with the collective pinning scenario. Instead, the $I_c^*(t)$ data unambiguously indicate a uniform local J_c in the bulk of the film, and a thin, higher J_c layer near the substrate. From the constant slope of $I_c^*(t)$, we calculated the local $J_c \sim 3.1\ \text{MA}/\text{cm}^2$ in the bulk of the film. The global $J_c(t) = J_{c0}(1 + t_0/t)$ thus increases as t decreases because of the very high

^{a)}Electronic mail: sikim@asc.magnet.fsu.edu

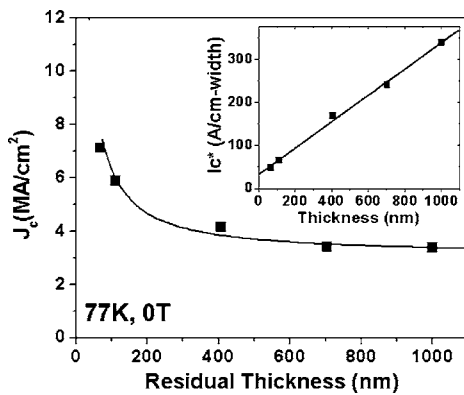


FIG. 1. Self-field 77 K $J_c(t)$ data as a function of the residual thickness after ion milling. The solid line represents $J_{c0}(t) = J_c(1) + t_0(t)$. The inset shows the critical current per unit width $I_c^*(0 \text{ T}, 77 \text{ K})$, which exhibits a linear dependence on t with a nonzero intercept at zero t .

$J_c(7.1 \text{ MA/cm}^2)$ of the 60–70 nm thick interface layer. The pinning structure in this highly defected interface layer will be addressed below.

The $J_c(H)$ at 77 K for different thicknesses are shown in Fig. 2(a). The overall shape of the $J_c(H)$ curves is rather insensitive to t , although the magnitude does increase at small t due to the high J_c interface layer. For comparison, $J_c(H)$ curves for a 280 nm YBCO film grown by PLD on a single crystal $(\text{La}_{0.30}\text{Sr}_{0.70})(\text{Al}_{0.65}\text{Ta}_{0.35})\text{O}_3$ (LSAT) substrate²⁴ and for 1 μm YBCO film grown by MOD on a single crystal yttrium-stabilized zirconia²¹ (YSZ) are also

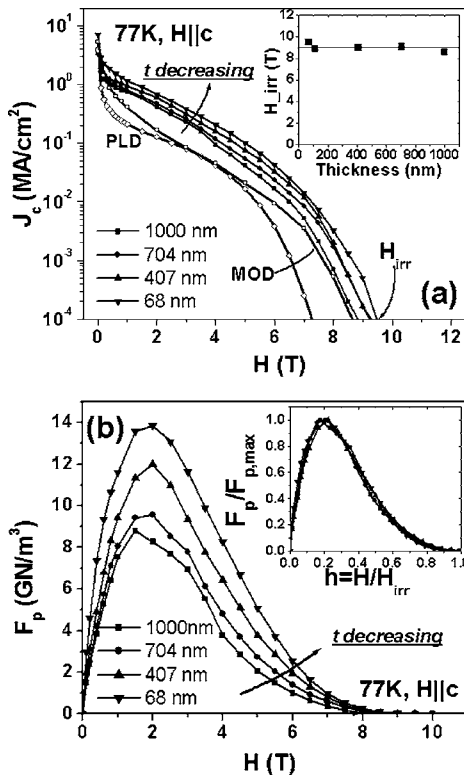


FIG. 2. (a) $J_c(H)$ at 77 K for different thicknesses. $J_c(H)$ curves for a 280 nm YBCO film grown by PLD on a single crystal LSAT substrate (Ref. 24) and for a 1 μm YBCO film made by MOD on a single YSZ crystal (Refs. 16 and 21) are shown for comparison. The inset shows the irreversibility field H_{irr} , determined at $J_c = 100 \text{ MA/cm}^2$, as a function of t . (b) Bulk pinning force plot $F_p(H)$ for different thicknesses. The inset shows that the normalized pinning force curves $F_p(H)/F_{p,max} = f(H/H_{irr})$ do not change as thickness changes.

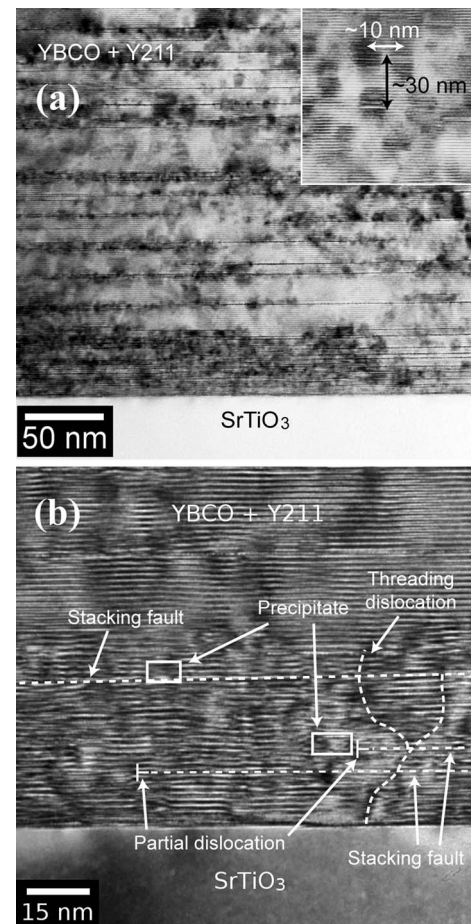


FIG. 3. (a) Cross-sectional TEM image shows a high density of randomly distributed Y211 nanoprecipitates. (b) Close-up view near the interface layer. Additional defects are present near the interface, especially higher density of stacking faults. (Some stacking faults, Y211 precipitates, and threading dislocations are labeled.) The YBCO matrix is highly distorted because of tangled stacking faults with Y211 precipitates and threading dislocations, producing high strain fields and lattice buckling.

shown. Neither the PLD nor MOD film had deliberately added second-phase particles, although the MOD films do have a complex pinning microstructure that contains pores, stacking faults, and Y_2O_3 particles. The strong vortex pinning of the present sample is quite evident. It results in much higher J_c values at all fields above a few tenths of a tesla, although the self-field J_c values of all three samples vary only from 3.4 to 5.3 A/cm^2 . The H_{irr} are essentially independent of t [inset of Fig. 2(a)], similar to what we found for the MOD film with strong pinning¹⁶ but quite different from the decreasing $H_{irr}(t)$ in the PLD film on LSAT.²⁴ The thickness-dependent bulk flux pinning force curves $F_p(H) = \mu H \times J_c(H)$ are shown in Fig. 2(b). The magnitude of the $F_{p,max}$ increases as t decreases because of the contribution of the strong-pinning interface layer. However, even at full thickness, $F_{p,max} = 8.8 \text{ GN/m}^3$ is more than two times higher than $F_{p,max} = 4.1 \text{ GN/m}^3$ for a 1 μm MOD film,^{16,21} while at the thinnest layer measured, $F_{p,max}$ of our samples reaches 13.8 GN/m^3 . However, the inset of Fig. 2(b) clearly shows that the normalized pinning forces $F_p/F_{p,max}$ plotted against the reduced fields H/H_{irr} are essentially independent of t , consistent with our conclusion that the pinning mechanisms are independent of t .

Figure 3 shows cross-sectional TEM images, which reveal a high density of Y211 precipitates (spheres with dark

contrast) and stacking faults (horizontal black lines). Typical sizes of the Y211 precipitates are $\sim 4\text{--}8$ nm [inset of Fig. 3(a)]; however, the effective pinning size including strain field is ~ 10 nm. As a result, the nominal volume fraction of the precipitates of ~ 5 vol % effectively increases to ~ 10 vol % if the strained regions are included. Within each thickness slice, the Y211 precipitates are rather randomly distributed in the YBCO, the average spacing being ~ 30 nm along the c axis and ~ 10 nm in the ab plane. [inset of Fig. 3(a)]. However, separation between the nanoprecipitates along the c axis may be smaller within the 60 nm interface layer where the stacking fault density is much larger than in the body of the film. It is shown in Fig. 3(a) that the Y211 tend to cluster and tangled with the stacking faults. Figure 3(b) also indicates that there are several threading dislocations, which are cut into short segments by the stacking faults, making a dense defect network near the interface, a structure which is consistent with the much stronger pinning near the interface.

Our experiment was motivated by the idea that the Y211 nanoprecipitates would provide strong 3D pinning so that vortices are chopped into separate, individually pinned segments.¹⁶ This condition is indeed fulfilled as indicated by the linear $I_c^*(t)$ behavior which implies a thickness-independent local J_c in the bulk of the film, and by the very high $F_{p,\max}$ of ~ 8.8 GN/m³ evaluated over the whole film thickness.

To check if these J_c values are consistent with the observed precipitate density, we estimated the maximum J_c which would be determined by depinning of elliptical vortex segments whose ends are fixed by neighboring nanoprecipitates with mean spacing d . The J_c can then be estimated from²⁵

$$J_c = \frac{\phi_0}{2\pi\mu_0\lambda_a\lambda_c d} \ln \frac{d}{\xi_c}. \quad (1)$$

Here, ϕ_0 is the flux quantum, μ_0 is the magnetic permeability, λ_a and λ_c are the London penetration depths in the ab plane and along the c axis, respectively, and ξ_c is the coherence length along the c axis. If we take $\lambda_a = 0.4$ μm , $\lambda_c = 2$ μm , and $\xi_c = 1$ nm at 77 K with the observed average mean Y211 separation d of ~ 30 nm, Eq. (1) gives $J_c \sim 3.7$ MA/cm², in agreement with the observed local J_c of ~ 3.1 MA/cm² away from the interface. The interface layer exhibits even stronger pinning where we expect an enhanced Y211 precipitate density. According to Eq. (1), the measured self-field J_c value of 7.1 MA/cm² at the interface layer implies a mean pin separation of ~ 10 nm, consistent with the smaller pin separation. Moreover, as shown in Fig. 3(b), the stacking faults have correlated partial dislocations tangled with the Y211 precipitates and the threading dislocations, producing strong strain fields, which may enhance the pinning further. This strong-pinning behavior with very high $F_{p,\max}$ of 13.8 GN/m³ reaches about two-thirds of the present champion samples made with the artificial pinning center distributions.^{5,6,26}

The production of uniform, dense arrays of nanoprecipitates is a natural route to a uniform through-thickness, vortex-pinning microstructure with very high and thickness-independent J_c . The significant potential of nanoscale pin-

ning engineering is well illustrated both by the results of this work and by the previous spectacularly high J_c values for the artificial pinning center structures.^{5,26} In the present case, ~ 5 vol % of insulating Y211 particles of $\sim 4\text{--}8$ nm, with separations of 10–30 nm, produce strong 3D pinning indeed.

This work was supported by the AFOSR-supported MURI “Critical Scientific Challenges of Coated Conductors” Contract No. F49620-01-1-0464.

¹T. Haugan, P. N. Barnes, R. Wheeler, F. Meisenkothen, and M. Sumption, *Nature* (London) **430**, 867 (2004).

²J. L. Macmanus-Driscoll, S. R. Foltyn, Q. X. Jia, H. Wang, A. Serquis, L. Civale, B. Maiorov, M. E. Hawley, M. P. Maley, and D. E. Peterson, *Nat. Mater.* **3**, 439 (2004).

³X. Y. Song, Z. J. Chen, S. I. Kim, D. M. Feldmann, D. Larbalestier, J. Reeves, Y. Y. Xie, and V. Selvamanickam, *Appl. Phys. Lett.* **88**, 212508 (2006).

⁴N. Long, N. Strickland, B. Chapman, N. Ross, J. Xia, X. Li, W. Zhang, T. Kodanandath, Y. Huang, and M. Rupich, *Supercond. Sci. Technol.* **18**, S405 (2005).

⁵M. Miura, Y. Yoshida, Y. Ichino, Y. Takai, K. Matsumoto, A. Ichinose, S. Horii, and M. Mukaida, *Jpn. J. Appl. Phys., Part 2* **45**, L11 (2006).

⁶J. Gutierrez, A. Llordes, J. Gazquez, M. Gibert, N. Roma, A. Pomar, F. Sandiumenge, N. Mestres, T. Puig, and X. Obradors, *Nat. Mater.* **6**, 367 (2007).

⁷S. R. Foltyn, P. N. Arendt, Q. X. Jia, H. Wang, J. L. MacManus-Driscoll, S. Kreiskott, R. F. DePaula, L. Stan, J. R. Groves, and P. C. Dowden, *Appl. Phys. Lett.* **82**, 4519 (2003).

⁸S. R. Foltyn, Q. X. Jia, P. N. Arendt, L. Kinder, Y. Fan, and J. F. Smith, *Appl. Phys. Lett.* **75**, 3692 (1999).

⁹S. R. Foltyn, P. Tiwari, R. C. Dye, M. Q. Le, and X. D. Wu, *Appl. Phys. Lett.* **63**, 1848 (1993).

¹⁰R. Feenstra, A. A. Gapud, F. A. List, E. D. Specht, D. K. Christen, T. G. Holesinger, and D. A. Feldmann, *IEEE Trans. Appl. Supercond.* **15**, 2803 (2005).

¹¹B. W. Kang, A. Goyal, D. R. Lee, J. E. Mathis, E. D. Specht, P. M. Martin, D. M. Kroeger, M. Paranthaman, and S. Sathyamurthy, *J. Mater. Res.* **17**, 1750 (2002).

¹²R. L. S. Emurgo, J. Z. Wu, T. Aytug, and D. K. Christen, *Appl. Phys. Lett.* **85**, 618 (2004).

¹³P. H. Kes and C. C. Tsuei, *Phys. Rev. B* **28**, 5126 (1983).

¹⁴A. Gurevich, *Superconductivity for Electric Systems 204 Annual Peer Review* (unpublished) (http://www.energetics.com/meetings/supercon04/pdfs/presentations/f_uw_coated_conductor_peer_rev_04final.pdf).

¹⁵S. R. Foltyn, H. Wang, L. Civale, Q. X. Jia, P. N. Arendt, B. Maiorov, Y. Li, M. P. Maley, and J. L. MacManus-Driscoll, *Appl. Phys. Lett.* **87**, 064521 (2005).

¹⁶S. I. Kim, A. Gurevich, X. Song, X. Li, W. Zhang, T. Kodanandath, M. W. Rupich, T. G. Holesinger, and D. C. Larbalestier, *Supercond. Sci. Technol.* **19**, 968 (2006).

¹⁷D. Dimos, P. Chaudhari, and J. Mannhart, *Phys. Rev. B* **41**, 4038 (1990).

¹⁸D. T. Verebelyi, D. K. Christen, R. Feenstra, C. Cantoni, A. Goyal, D. F. Lee, M. Paranthaman, P. N. Arendt, R. F. DePaula, J. R. Groves, and C. Prouteau, *Appl. Phys. Lett.* **76**, 1755 (2000).

¹⁹D. M. Feldmann, D. C. Larbalestier, D. T. Verebelyi, W. Zhang, Q. Li, G. N. Riley, R. Feenstra, A. Goyal, D. F. Lee, M. Paranthaman, D. M. Kroeger, and D. K. Christen, *Appl. Phys. Lett.* **79**, 3998 (2001).

²⁰N. F. Heinig, R. D. Redwing, J. E. Nordman, and D. C. Larbalestier, *Phys. Rev. B* **60**, 1409 (1999).

²¹S. I. Kim, D. M. Feldmann, D. T. Verebelyi, C. Thieme, X. Li, A. A. Polyanskii, and D. C. Larbalestier, *Phys. Rev. B* **71**, 104501 (2005).

²²Z. Chen, D. M. Feldmann, X. Song, S. I. Kim, A. Gurevich, J. Reeves, Y. Y. Xie, V. Selvamanickam, and D. C. Larbalestier, *Supercond. Sci. Technol.* (to be published).

²³M. Friesen and A. Gurevich, *Phys. Rev. B* **63**, 064521 (2001).

²⁴S. I. Kim, Z. Chen, A. Gurevich, F. Kametani, K.-J. Choi, C.-B. Eom, and D. C. Larbalestier (unpublished).

²⁵E. H. Brandt, *Phys. Rev. Lett.* **69**, 1105 (1992).

²⁶K. Matsumoto, T. Horide, A. Ichinose, S. Horii, Y. Yoshida, and M. Mukaida, *Jpn. J. Appl. Phys., Part 2* **44**, L246 (2005).